Available online at www.sciencedirect.com
ScienceDirect
European Journal of Mechanics B/Fluids 27 (2008) 309–321

Simulation of particles in fluid: a two-dimensional benchmark for a cylinder settling in a wall-bounded box

G. Pianet [a,*], E. Arquis [b]

[a] *Department of Chemical Engineering, École Polytechnique de Montréal, P.O. Box 6079, Stn. CV, Montréal, QC, Canada, H3C 3A7*
[b] *Laboratoire Transferts Écoulements Fluides Énergétique site ENSCPB, UMR CNRS 8508, 16, Av. Pey-Berland, 33607 Pessac, France*

Received 31 December 2006; received in revised form 1 June 2007; accepted 3 July 2007

Available online 21 July 2007

Abstract

This paper presents numerical experiments inspired by the theoretical work of Faxén for predicting the terminal velocity of a cylinder, settling halfway between two parallel walls at low Reynolds numbers. It is demonstrated that unexpected correlations exist between Faxén's results and the relaxation of a rigid disk initially suspended in a *wall-bounded* square box. To this end, the 1-Fluid (1F) method is used within a frame of Direct Numerical Simulation (DNS). In first place, the assessment of 1F method in two dimensions is presented. Simulations are in good agreement with Faxén's approach in half-bounded domains, and with simulation data from literature as well. Numerical experiments are then designed in order to investigate the transient behavior of a circular disk in a wall-bounded square box. Significant ranges of particle-to-wall containment ratios, density ratios and Galileo numbers were used in simulations. In the case where the aspect ratio belongs to the range [0.005,0.4] and the Galileo number is smaller than 1, it is found that the wall correction factor based on the *maximum* settling velocity could be correlated directly with the Faxén's correction factor based on the *terminal* settling velocity. For extreme values of containment, Faxén's theory gives irrelevant predictions, and alternative approaches based on 1F simulations are suggested. Finally, an original benchmark is designed as an efficient and inexpensive tool for validating numerical approaches to fluid/particle systems.

PACS: 47.55.Kf; 47.11.-j; 47.11.Df

Keywords: 1-Fluid model; DNS; Penalty method; Particles; 2D; Disperse flow; Numerical experiments; Cylinder drag; Benchmark

1. Introduction

The development of local numerical approaches to particulate flows requires early validation phases, and available references for both two- and three-dimensional systems. Furthermore, most of the DNS methods require a numerical assessment in two dimensions prior to the 3D implementation, which is sometimes much more complicated.

Two common ways of assessing fluid/particle interactions in planar coordinates are: (i) via the approach to axisymmetric flows around solids of revolution, (ii) via the analytical and theoretical analysis of flows around right circular cylinders. In case (i), the uniform motion of a sphere in the Stokes regime is well established (see [1–3]), and the

* Corresponding author.
E-mail address: gregoire.pianet@free.fr (G. Pianet).

0997-7546/$ – see front matter
doi:10.1016/j.euromechflu.2007.07.001

exact solution for the sphere drag has been widely used for assessing numerical approaches to particulate flows. The present study is concerned with case (ii). The first difficulty is related to the famous Stokes' paradox, which proves the non-existence of exact solutions for the cylinder drag in the creeping regime. Alternatively, solving the Oseen equations in which inertial contributions are introduced yields approximate solutions, such as the well-known result from Lamb [4], giving the cylinder drag in unlimited domains as a function of the Reynolds number. This is also the context in which the asymptotic expansion from Faxén (see [3]) succeeds in predicting the drag force on a cylinder moving between two parallel plane walls. One could also mention some experimental results from Huner and Hussey [5] for finite-length cylinders settling under gravity. The asymptotic behavior of the drag measured for vanishing Reynolds numbers was found to be compatible with Lamb's theory. Nevertheless, in all of these cases the geometry must be unbounded or at least half-bounded. Obviously, unbounded creeping flows are not well-suited for DNS. This originates in the long–range action of viscous effects and unappropriated boundary conditions that impose excessive domain sizes. For example, early simulations from Schlamp et al. [6] required domain sizes up to 1150 radii, for achieving negligible interactions between the particle boundary layer and domain boundaries. More recently, the asymptotic expansion from Faxén was verified numerically by several authors (see Liu et al. [7], Verhelst [8], Zisis and Mitsoulis [9]), and wall correction factors for a settling cylinder were studied using DNS by Ristow [10] in intermediate flow regimes.

The purpose of this paper is to build reliable correlations for a two-dimensional bounded problem. Results are designed in such a way that they could be used as an efficient and inexpensive benchmark for validating fluid/particle/wall interactions in numerical approaches. This analysis is achieved by the 1-Fluid method (1F), that was recently developed by Caltagirone and Vincent [11] and inspired by volume penalty methods in fictitious domains [12] and interface reconstruction [13]. The term 'one–fluid' means that fluid and solid phases are both considered as a single equivalent fluid in the sense of the Navier–Stokes equations. The equivalent fluid requires equivalent densities and viscosities, both depending on a phase function. The latter indicates whether the considered grid node belongs to fluid or solid phase, and drives the coupling of the Navier–Stokes equations with the interface transport equation. The 1F method has been validated before in both academic configurations and fully resolved three-dimensional multiphase problems (see [14–16]).

Next section describes the principles of 1F model and associated computational methods. The assessment section is dedicated to the simulation of a circular disk settling in half-bounded geometries. The effects of wall-bounded domains make the matter of the principal section, the one is compounded of three parts in which moderated, high and low containments are detailed. For each of these three zones, universal curves are proposed based on 1F simulations. All results are collected and rigourously tested in the last part for demonstrating a global correlation, which is then proposed as it provides a convenient base for a new fluid/particle benchmark.

2. Numerical method

2.1. Principles of the 1-Fluid model

The global technique consists of adding extra-terms to Navier–Stokes equations so that local modifications of equations are induced through *local* viscosities and densities $\mu_l(x, y, z, t)$ and $\rho_l(x, y, z, t)$. In that sense, the 1F method has similarities with the fictitious domain approach of Glowinski et al. [17] and with the Immersed Boundary Method of Peskin [18]. Great advantages are found by using a single Cartesian grid and by introducing the phase function $C(x, y, z, t)$ that matches the multiphase topology of the flow. So the dispersed phase is characterized by $C = 1$ and the continuous one by $C = 0$. It is consequently possible to express the local properties of the mixture as function of C, it is said basically: $\mu_l = \mu_f(1 - C) + \mu_p C$ and $\rho_l = \rho_f(1 - C) + \rho_p C$, where μ is the dynamic viscosity, ρ the density, the subscripts f and p pointing out respectively the fluid and solid phases. The latter one being considered like a fluid, it becomes necessary to set its viscosity as $\mu_p \to \infty$ so as to ensure a solid behavior. The final equations set reads the Navier–Stokes equations (Eq. (1)), an advection equation on the phase function (Eq. (2)), and the incompressibility constraint (Eq. (3)):

$$\rho_l\left(\frac{\partial \vec{u}}{\partial t} + (\vec{u}\cdot\nabla)\vec{u}\right) = \rho_l \vec{g} - \nabla p + \nabla\cdot\left(\mu_l(\nabla\vec{u} + \nabla^t\vec{u})\right), \tag{1}$$

$$\frac{\partial C}{\partial t} + \vec{u}\cdot\nabla C = 0, \tag{2}$$

$$\nabla\cdot\vec{u} = 0. \tag{3}$$

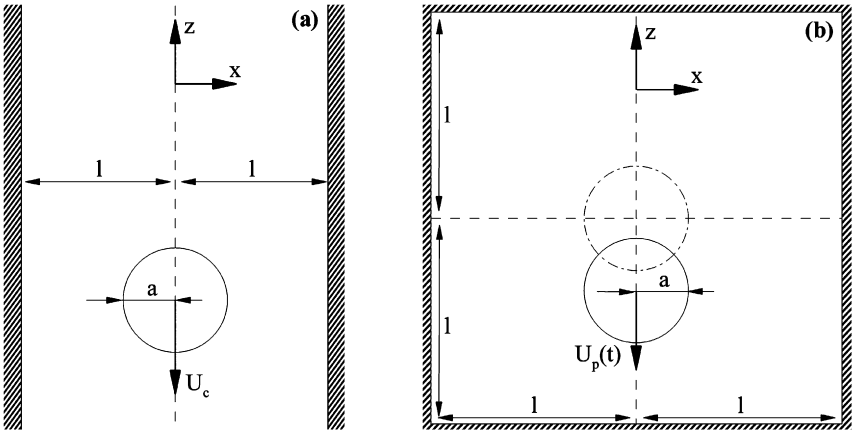

Fig. 1. (a): Definition sketch standing for Faxén's theory. (b): Definition sketch standing for the benchmark configuration.

2.2. Computational methodology

Solving Eq. (2) requires performant transport schemes to handle correctly the high gradients located on fluid–solid interfaces. To this end, a specific Volume Of Fluid scheme has been chosen and validated. The interface continuity between neighboring cells is ensured geometrically *via* explicit interface reconstruction (see the VOF–PLIC method of Youngs et al. [19]). Concerning the resolution of the Navier–Stokes equations, and in particular the velocity–pressure coupling, the method of the augmented Lagrangian [20] has been used. In order to satisfy the fluid incompressibility this technique have been adapted to multiphase flows by Vincent et al. [16]. The generalized augmented Lagrangian method is coupled with a viscosity penalty method [14,15] to ensure the solid phase undeformability. The discretization is achieved by means of an implicit finite volume method on a staggered mesh. All of the terms in Eq. (1) are spatially discretized using a second order accurate centered scheme. A second order accurate Gear scheme is applied for discretization in time. The algebraic system, resulting from the discretization of the various equations, is inverted by the iterative method BiCG–STAB [21].

3. Test-case based on a cylinder settling between two parallel plane walls

Preliminary assessment is based on the terminal settling velocity of an infinite cylinder of radius a released between two parallel planes situated at a distance of $2l$ from one another. Next is defined the Reynolds number based on particle–fluid relative velocity and cylinder radius, $Re = 2\rho_f U_{\text{rel}} a/\mu_f$. For the Reynolds number range investigated in this paper, $Re \leqslant \mathcal{O}(1)$, the system is two-dimensional, due to in-plane flow. The definition sketch in Fig. 1(a) defines the geometry in which one can use the Faxén's expansion (see [3]). Following the latter, one can approximate the *confined* terminal settling velocity U_c, as

$$U_c = (1-\rho)\frac{\rho_f\ g\ a^2}{4\ \mu_f}\ f(k_x), \quad \text{with}$$
$$f(k_x) = -0.9157 - \ln(k_x) + 1.7244k_x^2 - 1.7302k_x^4. \tag{4}$$

In these equations, $f(k_x)$ is the wall correction factor from the Faxén's theory, $\rho = \rho_p/\rho_f$ is the *particle* to *fluid* density ratio, and $k_x = a/l$ the dimensionless number associated to the *lateral* particle containment. Later, Faxén extended its analysis from powers of k_x^4 to powers of k_x^8 (see [9]). When $Re \leqslant \mathcal{O}(1)$ and $k_x \lesssim 1/4$, both approaches provide very accurate results for one cylinder fixed in a stream [7,9].

Besides, both readability and adaptability impose to make velocities dimensionless relative to the limit settling velocity of a cylinder in an unbounded fluid (i.e. $k_x = 0$). Stated as U_∞, it is computed starting from the Oseen and Lamb's formula for the cylinder drag (see [1]). Lamb's drag force per unit length is given as:

$$F_L = 4\pi\mu_f U_\infty \varepsilon_L, \quad \text{with}$$
$$\varepsilon_L = \left[1/2 - \gamma - \ln(Re_p/8)\right]^{-1}. \tag{5}$$

Table 1
Coefficient set used in Eq. (6)

i	0	1	2	3	4	5	6	7
α_i	2.0293	−0.90544	0.035955	0.0044292	3.695×10^{-4}	1.8872×10^{-5}	5.2736×10^{-7}	6.1472×10^{-9}

In Eqs. (5), $\gamma = 0.5772\ldots$ is the Euler's constant, and $Re_p = d_p \rho_f U_\infty / \mu_f$ the diameter-based particle Re number. The balance of forces is then considered at steady-state for calculating the unknown U_∞ by an iterative numerical approach. Alternatively, one suggest to replace the particle Reynolds number Re_p by the Galileo number $G_a = \frac{\rho_f}{\mu_f}\sqrt{|\rho - 1| g d_p^3}$. The latter has an equivalent physical sense in the present study, but with no explicit dependence to the velocity U_∞. One obtain the following approximated solution of Eq. (5):

$$U_\infty \simeq \frac{U_e}{\gamma} \sum_{i=0}^{n} \alpha_i \ln(G_a)^i, \quad \text{with}$$
$$U_e = \frac{2(\rho_f - \rho_p) g a^2}{8 \mu_f}. \tag{6}$$

It was found that the parameter set $n = 1$, $\alpha_0 = 2.00148$, $\alpha_1 = -1$ yields an acceptable approach to the Lamb's theory when $G_a < 1$. An alternative expansion made with the values reported in Table 1 yields a much better approximation with a relative discrepancy lower than 0.1% in the range $G_a \in [5 \times 10^{-10}, 1 \times 10^{0}]$. Beyond $G_a = 2$ the Lamb's theory is no more valid due to inertial effects.

For assessing the 1F method in the configuration from Fig. 1(a), numerical experiments are performed based on the following guidelines. The computational domain is set as a rectangle of height $2L = 40 d_p$ and width $2l = 4 d_p$. The boundary conditions upstream, downstream and on side walls are all modeled by a no-slip condition. For inlet and outlet boundaries, either free–slip or periodic boundary conditions have been tested but both were found inadequate. These drive the axial velocity to non-zero values as $(x, z) \to (0, \pm\infty)$. Setting walls on both ends is a relevant choice, considering the alternative situation of a cylinder fixed in a stream for which periodic or Neumann boundary conditions are common choices. Upstream or downstream boundary conditions should be different depending on whether the referential is attached to the laboratory or moving along with the particle.

The vertical particle containment $k_z^{-1} = L/a = 40$ was found small enough to prevent the particle from significant interaction with the top and bottom walls before the steady-state is reached. This statement satisfies the condition $k_z^{-1} > 30$ proposed by Liu et al. [7] for modelling an infinitely long channel. The containment $k_z^{-1} = 40$ is large enough to include the particle displacement occurring within the time it takes to reach a steady-state.

All of the simulations presented in this section were performed on a $N_x \times N_z = 100 \times 1000$ Cartesian grid. Following sections deal with the sensitivity of 1F method to various parameters.

3.1. Sensitivity to G_a and St numbers at constant particle containment

In this section the particle containment k_x is held fixed at the value $1/4$. Particle and fluid densities of reference are respectively fixed at $\rho_p = 3000$ [kg m^{-3}] and $\rho_f = 1000$ [kg m^{-3}]. Then the flow regime is modulated *via* the fluid viscosity μ_f. Resulting settling velocities $|U_c|$ are compared with Eq. (4).

From Fig. 2, excellent consistency is shown between analytical and numerical predictions. The relative error does not exceed 2% of the value of reference as G_a scales over three orders of magnitude (i.e. a five-order range in Re_p).

When $G_a > 5$, increasing discrepancies are noticeable, although simulations give some confidence (i.e. mass and momentum residuals keep very stable as G_a approach 5). Moreover, the same 1-Fluid code used for performing three-dimensional simulations of particulate flows has shown very good consistency with physical situations dominated by inertia (see Pianet et al. [14]). Thus the divergence between both approaches as Re_p exceeds unity originates in inertia, that Eq. (4) cannot predict, because actually it was not designed for.

In order to evaluate what effect the density ratio could have on the particle behavior, the Stokes number $St = \rho Re_p / 9$ is used as a one control parameter that compares the response time of the particle to the characteristic time associated with the flow field. Searching what combination of physical parameters yield a constant Reynolds number

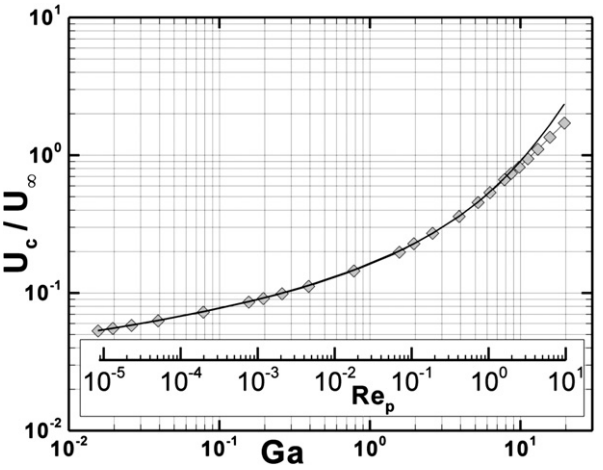

Fig. 2. Dimensionless settling velocity U_c/U_∞ versus Ga and Re_p. 1-Fluid simulations (diamonds), Faxén approximate solution (bold line, Eq. (4)), both relative to U_∞ from Eq. (6), at constant containment $k_x = 1/4$.

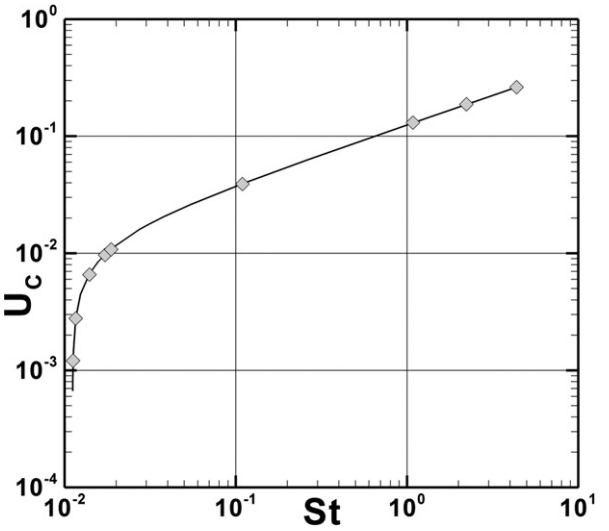

Fig. 3. Cylinder settling velocity U_c versus Stokes number S_t. 1-Fluid simulations (diamonds), Faxén approximate solution (bold line, Eq. (4)). $Re_p = 0.1$, $k_x = 1/4$.

for an arbitrary Stokes number requires to solve a set of second-order equations. Couples of solutions (μ_f, ρ_f) satisfy the following equation,

$$\rho_f = \frac{1}{2}\left[\rho_p \pm \sqrt{\rho_p^2 - \frac{8\mu_f^2 Re_p}{ga^3 f(k_x)}}\right]. \tag{7}$$

As suggested by Fig. 3, 1-Fluid simulations achieved with a Reynolds number $Re_p = 0.1$ and a containment $k_x = 1/4$ show no significant discrepancies with Faxén's approach (the maximum error does not exceed 1.5%). On the whole data set, the solid to fluid density ratio ranges between 1 and 400. So it is reasonable to conclude that in half-bounded domains, the cylinder drag does not depend on the Stokes number as long as other parameters stay within the bounds $k_x \leqslant 1/4$ and $Re_p \leqslant 0.1$.

Overall results show that 1F simulations and Faxén theory are in a convincing agreement over a wide range of particle Reynolds numbers $Re_p \in [0, 1]$ and Stokes numbers $St \in [0, 4]$. In further sections, simulation parameters are controlled so as to stand well within these limits.

3.2. Sensitivity to containment k_x with fixed fluid and particle properties

There is two possible methods for analyzing the impact of particle containment. Method (i): the domain size is fixed and the particle size is considered as a parameter. As $k_x \to 0$, the terminal velocity should decay to zero. When $k_x = 1$, there is no motion as the particle is blocked between the two planes. Method (ii): the particle size is fixed, while the gap between the two planes is modulated. The difference with the case (i) as $k_x \to 0$, is that the terminal velocity U_c increases steadily to the terminal settling velocity U_∞ (i.e. without walls). The purpose of this section is to study the Faxén approach in the range $k_x \in [0, 1]$, then to test the 1-Fluid method where the theoretical approach is known to be valid. The present section focuses on case (i), which means that both domain size and spatial resolution are set as constants and the particle radius a is modulated.

In Fig. 4 is shown a good agreement between 1F simulations and every Faxén's approximation for values of containment k_x ranging from 0 to 0.25. Here, the relative discrepancy ε never exceeds a few percents, the first simulation excepted ($k_x = 0.02$ with $\varepsilon \simeq 50\%$). This is due to the excessively low particle resolution, $d_p = 3\delta_x$, reading δ_x as the unit of grid length. Fig. 5 details the convergence of the case $k_x = 0.02$. The four plotted points correspond respectively to $d_p = 3,\ 4,\ 5$ and $8\delta_x$. When the relative error ε is plotted against the particle area expressed in units of grid surface $N_a = \pi a^2/\delta_x^2$, the spatial convergence to the analytical value is made clear with an order 1.3. This is a feature

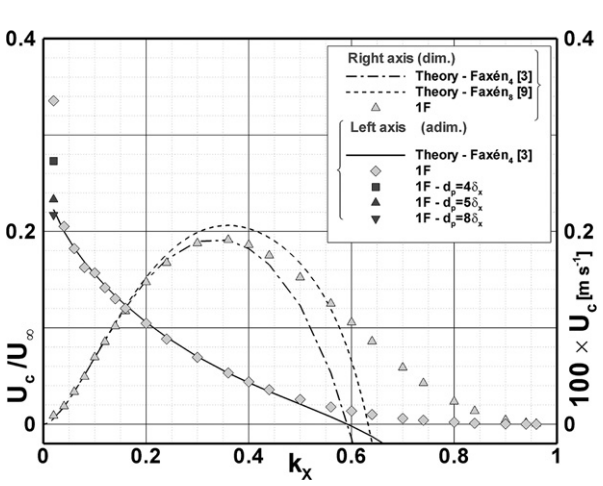

Fig. 4. Cylinder settling velocity U_c versus lateral particle containment. 1-Fluid simulations, 4th and 8th order solutions from Faxén (see [3,9]).

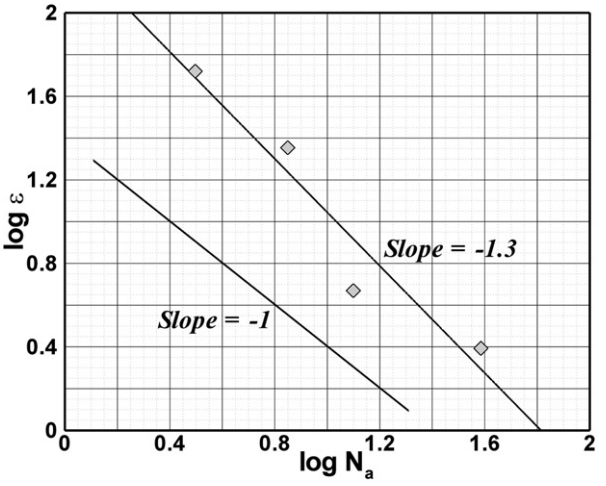

Fig. 5. Spatial convergence of 1-Fluid simulations to Faxén's 4th order solution (see [3]). $k_x = 0.02$. Natural logarithm of the relative error ε *versus* the particle area N_a expressed in units of cell surface.

proper to the 1F method [14], in which the order in space is relatively low, but balanced by the high level of precision at very low resolutions. Quantitatively good results are found starting from 5 grid points in the particle diameter, and $d_p = 9\delta_x$ is sufficient for achieving a relative error lower than 1%. Of course, these results must be discussed for significant Reynolds numbers ($Re_p > 1$) for which the thinner boundary layer requires to increase spatial resolution on the interface.

In the range $k_x \in [0.25, 0.4]$, 1F simulations clearly converge to the original Faxén's 4th order approximation, and a discrepancy with the later 8th order approximation is observed. As aforementioned, several authors have treated similar cases before, in which cylinders are fixed and their boundaries well discretized thanks to high–resolution adapted grids. Quantitative comparisons are presented in Table 2 between 1F method, Faxén's approximations, and numerical simulations from Liu et al. [7] or Zisis and Mitsoulis [9]. Corresponding velocity time series can be seen in Fig. 6 showing how steady-state is reached. Note that for the smallest containment, the characteristic time of stabilization $\tau_{95\%}$ is significantly increased.

In the range $k_x \in [0, 0.25]$, excellent agreement is found between all approaches, even though this study was not intended to achieve the same levels of accuracy as those from the other two numerical approaches. For small containments their results [7,9] clearly converge to Faxén's 8th order approximation. Nevertheless this trend in their data is rather questionable when $k_x > 0.25$, since they only show a single point at $k_x = 0.5$. With no doubt, one can conclude that all Faxén's approximations can be used with confidence for $k_x \in [0, 0.25]$. From 1F results or the ones from literature, the divergence predicted beyond $k_x \sim 0.4$ is confirmed. In the following sections the Faxén's 4th order approximation has been chosen, referred later as 'Faxén's theory' for simplicity. This choice has been made considering that the case of a moving cylinder may differ slightly from the case of a fixed one. Moreover, the present approach is a DNS, so there is no reason to loose accuracy when increasing the containment, as long as the spatial discretization is sufficient. What is shown on right axis of Fig. 4 is that the original 4th order approximation is the less accurate, but is acceptable over a wider range of containment and clearly best suited to the purpose of this paper.

By analyzing 1F predictions for the whole range of containment $k_x \in [0, 1]$, the non-normalized velocity series U_c is compounded of three distinct zones (see Fig. 4). In the first one, the settling velocity growth depends mostly on buoyancy forces. The second zone is found where the velocity is quite insensitive through changes in containment, a behavior that originates from balanced contributions of buoyancy and friction forces (in other words, when a change in particle radius Δa does not affect significantly the equilibrium $\Delta F_{\text{buoyancy}} \simeq -\Delta F_{\text{friction}}$). Although Faxén's 4th order approximation diverges strongly starting from $k_x = 0.4$, 1F approach yields the same maximum location $k_x \simeq 0.35$ as well. In the third zone, friction forces are predominating ($\Delta a \to \Delta F_{\text{friction}} > \Delta F_{\text{buoyancy}}$) and drive as expected a slow decay of the particle velocity to zero.

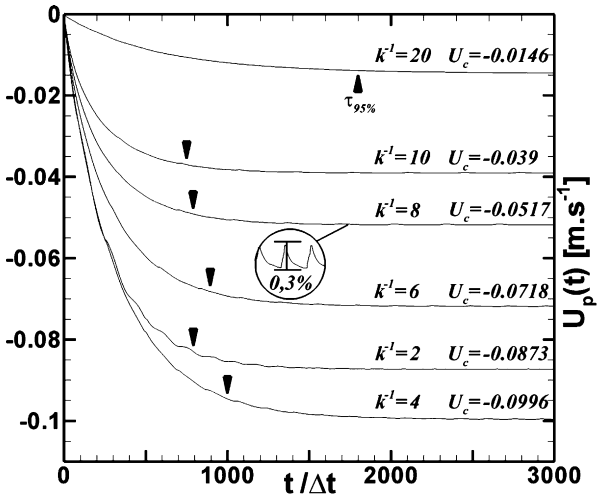

Fig. 6. Velocity time series of a cylinder moving between two parallel plane walls. (See corresponding data set from Table 2.) $U_p(\tau_{95\%}) = 0.95 \times U_c$. Simulation data: $\Delta t = 1.10^{-4}$ [s], $d_p = 10\delta_x$, $l = 0.1$ [m], $\rho_p = 3000$ [kg m^{-3}], $\rho_f = 1000$ [kg m^{-3}], $\mu_f = 17.52$ [Pa s].

Table 2
1-Fluid simulations vs. literature data for the normalized cylinder drag* F_N. Faxén's 4th and 8th order approximation, and relative error with simulations from 1F method, Liu et al. [7], and Zisis and Mitsoulis [9]

k^{-1}	F_N^4	F_N^8	% diff.	% diff.	% diff.	% diff.
	Faxén (see [3,9])		F_N^{1F}/F_N^4	F_N^{1F}/F_N^8	$F_N^{\text{Liu [7]}}/F_N^8$	$F_N^{\text{Zisis [9]}}/F_N^8$
1 : 2	187.73	138.49	19.49	9.14	4.44	4.46
1 : 4	32.976	31.943	0.43	3.68	0.002	0.04
1 : 6	20.430	20.148	0.06	1.33	0.007	–
1 : 8	15.836	15.713	0.65	1.44	0.002	0.06
1 : 10	13.426	13.359	0.76	1.27	0.007	0.07
1 : 20	9.0434	9.0321	0.06	0.06	0.001	0.07

* $F_N = 6\pi\mu_f U_c / f(k_x)$.

4. Test-case based on a cylinder settling in a bounded geometry

In the last section, it has been shown that the Faxén analysis could be used with success for validating particle/fluid/wall interactions in two dimensions. As stated before, this requires half-bounded domains that involve approximations at the simulation level, for modelling both upstream and downstream boundary conditions. In the present section, an attempt is given to build correlations between the terminal velocity U_c computed from Eq. (4) and the maximum particle velocity $U_p^m = \max(U_p(t))$ predicted in the bounded case, defined in the sketch from Fig. 1(b).

4.1. Simulation settings

Further simulations are performed respecting the method (ii), in which the particle radius is held fixed and the domain size is considered as a parameter. The transient particle velocity noted $U_p(t)$ is compared to the settling velocity U_∞ of a cylinder in an unbounded fluid. Let the dimensionless maximum particle velocity in time be U_p^m / U_∞, a value that can range theoretically from 0 to 1. In the present study, particle behavior is analyzed over three ranges of containment ($k_x = k_z = k$), respectively defined as low ($k < 0.005$), intermediate ($k \in [0.005, 0.83]$), and high ($k > 0.83$). The intermediate containment is investigated on regular Cartesian grids, subsequently designated as $M1$ grids. Low and high containment are simulated on two types of exponential grids. The $M2$ type for high containment is refined in the interstitial zone between the wall and the particle. The $M3$ type for low containment is refined so as to increase the resolution in the particle boundary layer. The three grid types are schematized in Fig. 7. In this

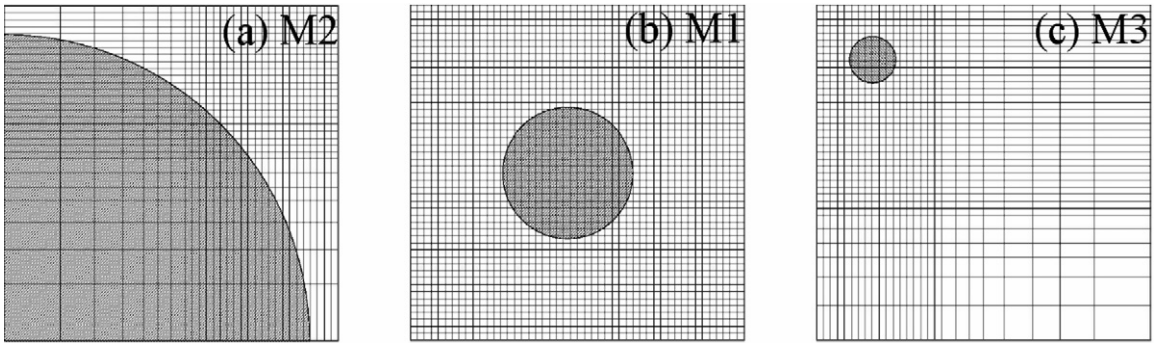

Fig. 7. Mesh design for a specific particle containment range. From left to right: (a) high containment ($k \to 1$, grid type $M2$), (b) intermediate containment ($0 < k < 1$, grid type $M1$), (c) low containment ($k \to 0$, grid type $M3$).

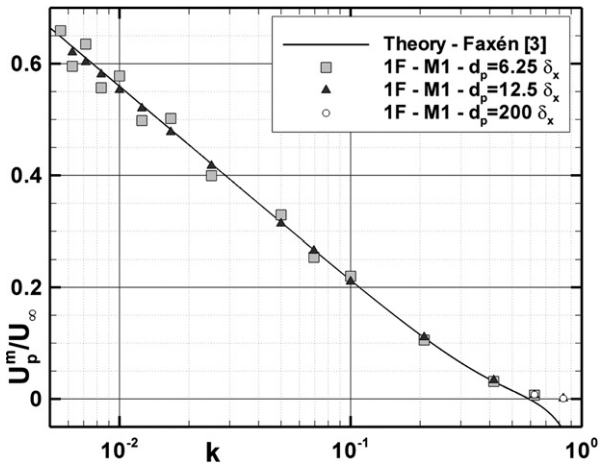

Fig. 8. Semi-logarithmic plot of the cylinder maximum velocity U_p^m/U_∞ in the square box configuration. Faxén's theory, 1-Fluid simulations with $M1$ grid type. Effect of spatial resolution $d_p = 6.25$, 12.5 and 200 δ_x.

section, the following physical properties are fixed: $\rho_p = 3000$ [kg m^{-3}], $\rho_f = 1000$ [kg m^{-3}], $\mu_f = 10$ [Pa s] and $a = 2.5\ 10^{-3}$ [m].

The comparison with Faxén's relation requires particular precautions: when measuring U_p^m, the unsteady contribution to the particle acceleration must be *vanishing*. In other words, U_p^m is measured when $U_p(t)$ presents an asymptote before decaying to zero. In case of instantaneous *maxima* before deceleration, the simulation is rejected and performed again with a reduced time-step or different input data. Obviously, some particular sets of input parameters drive results that cannot fulfill all of these conditions as well. These are then used for restricting the validity range of suggested correlations.

4.2. Results

(i) *moderate containment* (*M1*):

The domain size is modulated as k is given values from 0.005 to 0.83. The sensitivity to spatial resolution is tested through several particle resolutions $d_p = 6.25,\ 12.5$ and 200 δ_x. This is done to highlight data shifts occurring where resolution does play an important role. The dimensionless velocity (in fact the wall correction factor) U_p^m/U_∞ from 1F method, and the Faxén's approximation U_c/U_∞ for half-bounded domains, are both compared on Fig. 8. Very surprisingly, the 1F method and the Faxén's approach collapse together on a single curve, as k ranges from the lower bound 0.005 up to the value 0.4 which was previously given as the validity limit of the Faxén's theory. This interesting property is probably restricted to creeping flows – in the present case, $Re_p \leqslant 0.01$ and $St \leqslant 0.002$ – but more attention will be addressed to this problem later in the paper.

For interpreting the physical meaning of these results, one can suggest that the influence of lateral containment overwhelm the vertical one, since the generated backflow intensity depends mostly on k_x. The point is that the time during which the particle accelerates is very small compared to the characteristic time of particle displacement (hypothesis of small Stokes numbers), so the particle-wall gaps could be considered as equal and constant during acceleration. As a consequence of both vertical motion and symmetrical configuration, the forces due to the top and bottom walls are mainly related to pressure, and these lubrication forces of equal intensity but opposite direction cancel each other. On both sides of the cylinder the flow (the backflow in fact) is completely different, there is significant forces applied on particle interface, mostly related to friction. The hypothesis of a direct dependence between the particle velocity and the backflow intensity could explain such results for high k_x values.

The spatial convergence to Faxén's approach leave no doubt. With only 6.25 grid units δ_x in the particle diameter, the 1F method is oscillating around the reference value with an amplitude of roughly 4%. The oscillation is a numerical artifact due to the particle interface, which is alternatively placed on or between grid nodes. This artifact is visibly damped when using $d_p = 12.5\ \delta_x$. As k tends to zero, 1F estimation seems to diverge very slightly from the analytical value. This was expected at a fixed particle radius and $l \to \infty$, since the terminal velocity obtained with Eq. (4) is diverging to infinity instead of converging to U_∞. Beyond this point, the spatial resolution required in case of a $M1$ grid type becomes too expensive to make the discrepancy clear. Faxén's law limitations also appear as k tends to 1. The predicted 1F velocity obviously vanishes, but in the same way as before a mesh refinement is required for justifying potential correlations.

(ii) *high containment* (*M2*):

Fig. 7 points to how $M2$ grid type is made such as to improve spatial resolution in the gap $g_{pp} = l - d_p/2$ between the particle and walls. One may note that mesh refinement is increased in fluid in the directions subjected to the strongest velocity gradients. Inhomogeneities in space and time for the mesh inside the particle have little importance. In fact the interesting particle's relaxation phase is quasi–instantaneous with high k values, so there is no significant interface displacement during this time. 1F results range from $k = 0.625$ to $k = 0.98$. Starting from $k > 0.4$, Fig. 9 compares $M2$ and $M1$ simulations with the half-bounded approximation from Faxén. Confidence is given in the $M2$ choice by looking $M1$ results for different resolutions in space: indeed it is found that increasing the containment parameter k from 0.625 to 0.833 yields a strong decrease in convergence velocity (convergence in space changes from 1.3 to 0.9). Based on these results, an extrapolation is done by weighting alternatively the curve by $M1$ data when $k < 0.7$, then by $M2$ data when $k > 0.7$. The resulting law is proposed in Eq. (8) with Table 3. It is naturally builded as a function of the non-dimensional particle-wall gap $[1 - k] = g_{pp}/l$. Following what was mentioned earlier, the flow picture at $k = 0.962$ (see Fig. 10) shows an example of the dominating lateral friction effects over the vertical ones.

$$U_p^m / U_\infty = \sum_{i=1}^{2} \alpha_i (1-k)^{2.8i}, \quad k > 0.4, \tag{8}$$

$$U_p^m / U_\infty = 1 - \sum_{i=1}^{3} \alpha_i k^{1/2^i}, \quad k < 0.01, \tag{9}$$

(iii) *low containment* (*M3*):

Low-containment simulations are rather problematic on two levels: On the one hand, the resolution in space required for modelling a particle in large domains involve prohibitive costs (quantitatively, changing k from $k = 5 \times 10^{-3}$ to $k = 5 \times 10^{-4}$ yields an increase from $800K$ to $80M$ grid points at a resolution $d_p = 6.25\ \delta_x$). On the other hand, the characteristic time of sedimentation $\tau_{95\%}$ (i.e. when 95% of the terminal velocity is obtained) increases as the containment decreases, proportionally to the time it takes for the boundary layer to develop over the domain and stabilize (the following tendency was observed in 1F simulations: $\tau_{95} \propto 1/\sqrt{k}$ as $k \to 0$). Since simulations on classical grids are expensive in both time and memory, the $M3$ grid type is used to investigate lower containments with domain sizes up to 10.000 particle diameters.

Unlike the Faxén's approach, 1F simulation does not result in an inconsistency when decreasing the particle containment. Fig. 11 shows that 1F method predicts a very slow but effective asymptotic behavior, towards the cylinder

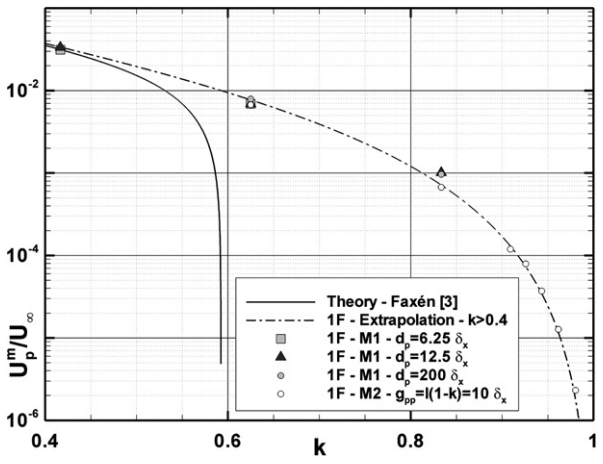

Fig. 9. Plot of the cylinder characteristic velocity U_p^m/U_∞ in the square box configuration. Asymptotic behavior as k is approaching unity. Faxén's theory, 1-Fluid simulations $M1$, $M2$ and numerical extrapolation from Eq. (8).

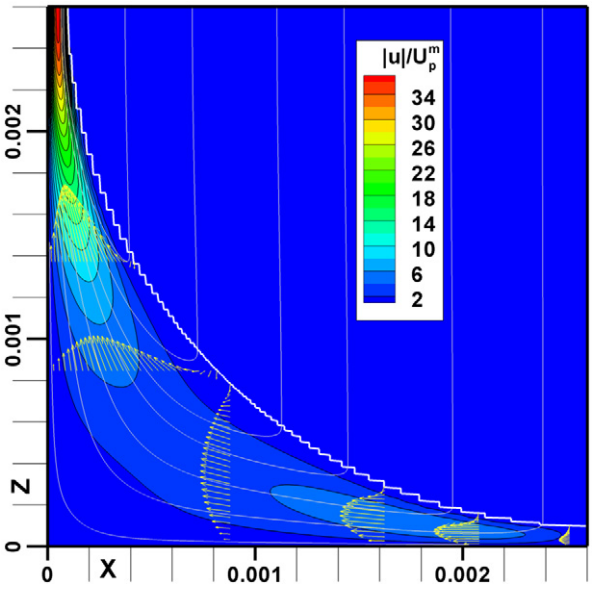

Fig. 10. Flow field for $k = 0.962$, $M2$ mesh, magnitude of the velocity field $|u|/U_p^m$, stream lines, vector samples in fluid and interface position indicated by isovalue $C = 0.5$.

Table 3
High containment approach $k > 0.4$ (see Eq. (8))

i	1	2
α_i	0.1068	0.2044

Table 4
Low containment approach $k < 0.01$ (see Eq. (9))

i	1	2	3
α_i	4.639	−1.448	0.7863

velocity in unlimited fluid. A relation for extending the Faxén's law below $k = 0.01$ is proposed in Eq. (9) related with data from Table 4.

In addition, it must be noticed that the linear approach[1] due to Ristow [10] differs strongly from both 1-Fluid method and Faxén's approach, since its convergence to U_∞ occurs far too early. The strong discrepancy should be explained by differences in flow regime with increased inertial effects, since Ristow's model converges much easily to the unbounded terminal velocity. This faster convergence should originate in a lower dependency to containment k and a more limited momentum diffusion.

Concerning 1-Fluid method with the $M3$ grid, numerical problems appear as the particle boundary layer develops beyond the regular part of the $M3$ grid, inducing unphysical feedbacks at the particle velocity level and uncertainty on the steady-state measurement. This is why no more data for $k < 1 \times 10^{-4}$ could be presented, mostly because a huge investment in computing power is needed for quite insignificant changes in results, in regard of 1F predictions for the very slow decay of the correction factor.

Finally, one seeks to assess the velocity field prediction as k vanishes. Within the Lamb's theory framework, the following formula is given for approaching the two-dimensional velocity distribution around a fixed cylinder at $Re_p \lesssim \mathcal{O}(1)$ (see [1]):

$$\mathbf{u} = \mathbf{U}_\infty + 2\varepsilon_L \mathbf{U}_\infty \left(-\frac{1}{2}\log\left(\frac{r}{a}\right) - \frac{1}{4} + \frac{1}{4}\frac{a^2}{r^2} \right) + 2\varepsilon_L \mathbf{z} \frac{(\mathbf{U}_\infty \cdot \mathbf{z})}{r^2} \left(\frac{1}{2} - \frac{1}{2}\frac{a^2}{r^2} \right). \tag{10}$$

With the parameters $k = 1 \times 10^{-4}$ and $Re_p = 0.0086$, the numerical approach gives a maximum velocity $U_p^m/U_\infty = 85.3\%$. The discrepancy of 15% is not negligible, so the velocity magnitude M_{sim} is corrected along

[1] $U_p^m/U_\infty \simeq 1 - 1.18k$.

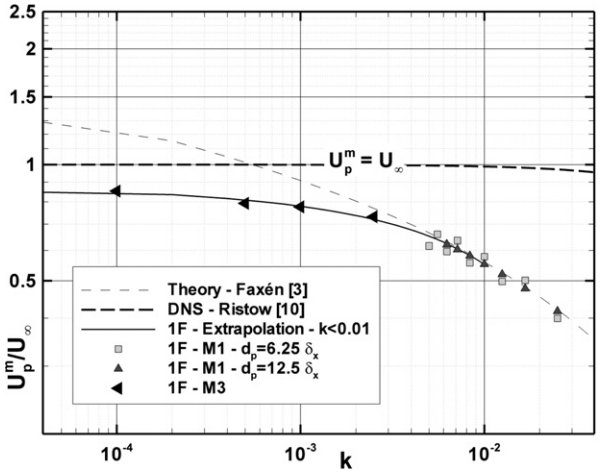

Fig. 11. Asymptotic behavior of the cylinder characteristic velocity U_p^m/U_∞ in a square–box, as the containment k vanishes. Faxén's theory, DNS (see Ristow [10]), 1-Fluid simulations $M1$, $M3$ and numerical extrapolation from Eq. (9).

the direction perpendicular to the particle motion following the substitution $(1 - M_{\text{sim}}) \leftarrow (1 - M_{\text{sim}})/1.325$. Fig. 12 focuses successively on the near-field surrounding the particle. In the particle vicinity, isotropic matching is noticed between simulation and theory. Both velocity fields are similar in shape and value. The scale offset found with velocities in unbounded domains was easily compensated by a simple linear correction. This correction probably scales with the wall correction factor. From Fig. 12, discrepancies and loss of upstream/downstream symmetry are noticeable at a distance r of the order of a/Re_p. Beyond that distance, asymmetry is something one can expect from DNS, because inertial effects are no more negligible compared to viscous ones. Finally, this gives good confidence to the 1-Fluid method and subsequent results for constrained simulations.

4.3. Benchmark setup and validation

All results presented before must now be tested over a wide range of configurations, in order to check in what conditions the preceding correlation does depend on the sole particle containment k. To do so, random values are affected to physical parameters. Either settling or raising particles are allowed since ρ_p and ρ_f can range between 100 and 1000 $\text{Kg}\,\text{m}^{-3}$. The fluid dynamic viscosity μ_f is assigned values ranging between 1 and 10 Pa s. Four sets are chosen randomly for each value of containment k, varying itself between 0.01 and 0.6. All simulations were performed on regular $M1$ grids with a constant particle resolution defined as $d_p = 10\ \delta_x$. The side length of the domain, $2l$, is constant so k is modulated through changes in particle radius a. As a consequence the resolution in space is $\delta_x = 2lk/10$. All boundary conditions are set as no-slip conditions and the particle is released at rest from the center of the square-box. Fig. 13 details the distribution of the data sets $(\rho_p/\rho_f, G_a)$ used in simulations. Fig. 14 summarizes the final result: it compares the wall correction factor f to the particle containment k. f is calculated following $f = F_{1F}/F_L$, where $F_{1F} = 4\pi\mu_f U_p^m$ is the drag force per unit length measured using 1-Fluid simulations, and F_L the one from Lamb's theory (see Eq. (5)). It is shown that f compares directly to the Faxén's correction factor from Eq. (4). The correction factor calculated with the 1-Fluid method and the Faxén factor collapse together on a single universal curve. The models from Eqs. (8) and (9) and a dataset from $M1$ configurations are also indicated, since they were used as references for calculating the relative error: $\varepsilon = 100 \times |f_{\text{rand}} - f_{\text{ref}}|/f_{\text{ref}}$ [%].

Fig. 13 also details the global error level. Just four points from Fig. 13 are not represented since they drive relative errors greater than 50%. All the data sets satisfying $G_a < 1$ yield acceptable results. The combination of buoyant or raising particles at $k > 0.3$ and flow regimes $G_a > 1$ drives generally an augmentation in the relative error level. This may be because the raising motion is potentially more sensitive to inertia and containment. To sum-up, with the conditions $\mathbf{G_a < 1}$ and $\mathbf{0.01 < k < 0.3}$, it was shown that the drag on a cylinder settling in a bounded box could be correlated accurately with the drag of the same cylinder settling between two infinite parallel walls.

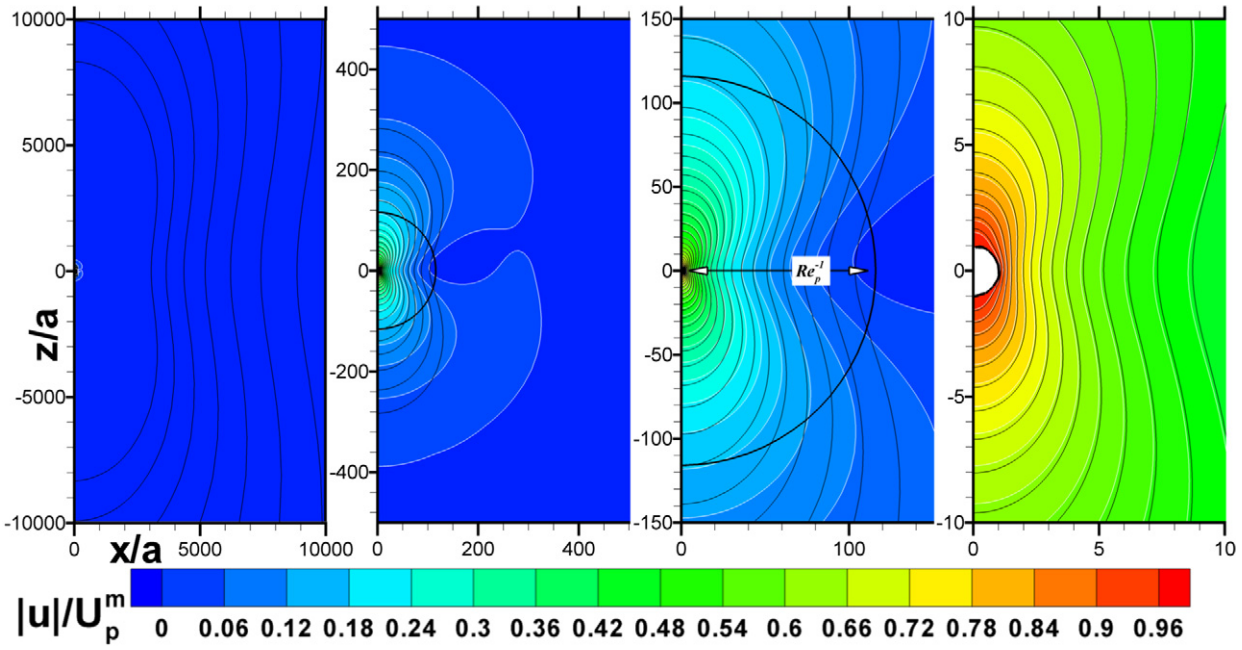

Fig. 12. Flow field in a quasi-unlimited domain. $M3$ grid, $k = 1 \times 10^{-4}$, $Re_p = 0.0086$. Successive focuses on the vicinity of the particle, whose center and radius a have been used for scaling the axes of reference. White and colored contour levels of the velocity field magnitude $|u|/U_p^m$ (simulation), black contour levels for the analytical solution (Eq. (10), see [1]). Limit $r/a = Re_p^{-1}$ of negligible inertial effects (black circle).

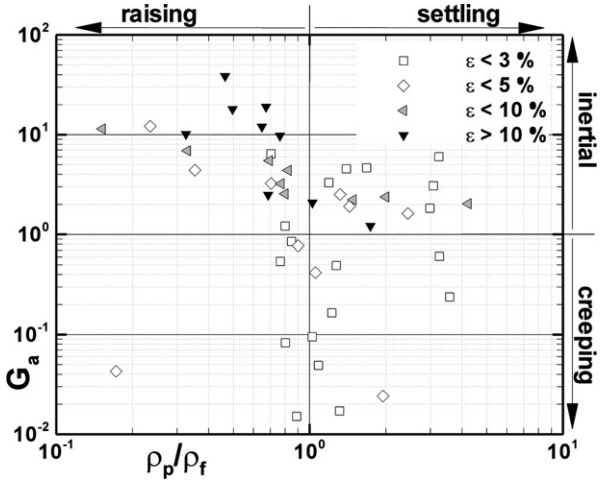

Fig. 13. Random distribution of benchmark parameters, expressed by combinations of Galileo number and solid to fluid density ratio. Relative error ε estimated from the benchmark results.

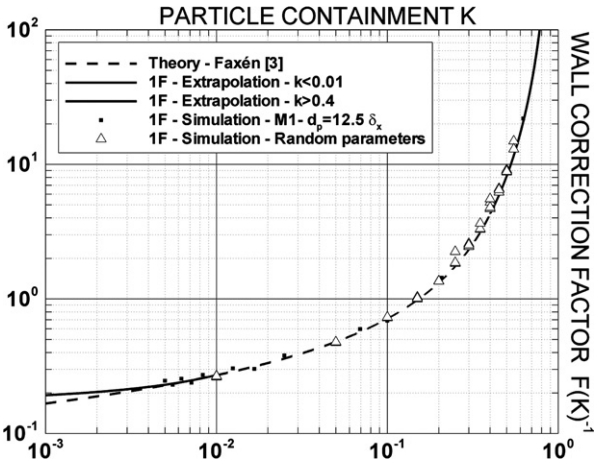

Fig. 14. Results based on random benchmark parameters. Faxén's analytical reference, correlations from Eqs. (8) and (9) and previous $M1$ results

5. Conclusion

This paper was intended to investigate the case of a cylinder settling inside a bounded box in the creeping regime, with a view to build a reliable fluid/particle benchmark in two dimensions. By using a Direct Numerical Simulation approach classified as a one-fluid method, it was demonstrated that classical in-plane situations could be reproduced numerically. Used as a reference, analytic formulations from literature were given to quantify the drag force on a cylinder moving within unlimited or half-bounded domains. A particular attention was given to the development from Faxén concerning a circular disk moving between infinite sidewalls. The development in question was systematically

tested and criticized, and its zone of validity was situated with success. The case of the bounded box was then presented in three parts relative to three consecutive particle containment ranges. The central demonstration is that the half-bounded approach from Faxén could be transposed directly to bounded situations. As this was shown to be available only for intermediate containments, the extremes situations were simulated with particular grids. Numerical results were used to provide extrapolations in the continuity of the Faxén approach. The last section was a drastic testing of preceding assertions, performed through almost fifty simulations in which all physical inputs were defined randomly. This allowed two results: on the one hand, previous assertion was comforted with good accuracy; on the other hand, the good amount of simulations provided some informations about the limits inside which the correlation is available.

Finally the objectives were fulfilled as a reliable benchmark is proposed. This test-case could be attractive for several reasons: (i) all of the fluid/particle/wall interactions are involved, (ii) all boundary conditions are no-slip conditions that can be implemented exactly, (iii) both intermediate containments and two-dimensional configurations are features that allows the problem to be simulated very quickly on small grids. Future objectives would lie in checking the benchmark result with some local approaches such like Lattice–Boltzmann, Arbitrary Lagrange–Euler methods, Distributed Lagrange Multipliers or Stokes solvers. Finally one improvement would be – if possible – to propose a unique wall correction factor over the range $k \in [0, 1]$.

Acknowledgements

We wish to acknowledge the National Computer Centre of Higher Education (C.I.N.E.S) in Montpellier (France), and the Institute for Development and Resources in Intensive Scientific computing (I.D.R.I.S) in Orsay (France), for providing the computing facilities used for the simulations presented in this paper.

References

[1] G.K. Batchelor, An Introduction to Fluid Dynamics, Cambridge University Press, Cambridge, 1967.
[2] H. Brenner, The slow motion of a sphere through a viscous fluid towards a plane surface, Chem. Eng. Sci. 16 (1961) 242–251.
[3] J. Happel, H. Brenner, Low Reynolds Number Hydrodynamics, Kluwer Academic Publishers, London, 1983.
[4] H. Lamb, On the uniform motion of a sphere through a viscous fluid, Philos. Mag. 21 (1911) 112–121.
[5] B. Huner, R.G. Hussey, Cylinder drag at low Reynolds number, Phys. Fluids 20 (8) (1977) 1211–1218.
[6] R.J. Schlamp, H.R. Pruppacher, A.E. Hamielec, A numerical investigation of the efficiency with which simple columnar ice crystals collide with supercooled water drops, J. Atmos. Sci. 32 (12) (1975) 2330–2337.
[7] A.W. Liu, D.E. Bornside, R.C. Armstrong, R.A. Brown, Viscoelastic flow of polymer solutions around a periodic, linear array of cylinders: comparisons of predictions for microstructure and flow fields, J. Non-Newtonian Fluid Mech. 77 (3) (1998) 153–190.
[8] J. Verhelst, Model evaluation and dynamics of a viscoelastic fluid in a complex flow, PhD Thesis, Technische Univerisiteit Delft, Delft University Press, 2001.
[9] T. Zisis , E. Mitsoulis, Viscoplastic flow around a cylinder kept between parallel plates, J. Non-Newtonian Fluid Mech. 105 (2002) 1–20.
[10] G.H. Ristow, Wall correction factor for sinking cylinders in fluids, Phys. Rev. E 55 (3) (1997) 2808–2813.
[11] J.P. Caltagirone, S. Vincent, Sur une méthode de pénalisation tensorielle pour la résolution des équations de Navier–Stokes, C. R. Acad. Sci. Paris, Sér. IIb 329 (2001) 607–613.
[12] K. Khadra, P. Angot, S. Parneix, J.P. Caltagirone, Fictitious domain approach for numerical modelling of Navier–Stokes equations, Int. J. Numer. Meth. Fluids 34 (1) (2000) 651–684.
[13] R. Scardovelli, S. Zaleski, Direct Numerical Simulation of free-surface and interfacial flow, Annu. Rev. Fluid Mech. 31 (1) (1999) 567–603.
[14] G. Pianet, A. Ten Cate, J.J. Derksen, E. Arquis, Assessment of the 1–fluid method for DNS of particulate flows: Sedimentation of a single sphere at moderate to high Reynolds numbers, Comput. & Fluids 36 (2) (2006) 359–375.
[15] N. Randrianarivelo, G. Pianet, S. Vincent, J.P. Caltagirone, Numerical modelling of the solid particles motion using a new penalty method, Int. J. Numer. Meth. Fluids 47 (10–11) (2005) 1245–1251.
[16] S. Vincent, J.P. Caltagirone, P. Lubin, N. Randrianarivelo, An adaptative augmented Lagrangian method for three-dimensional multi-material flows, Comput. & Fluids 33 (10) (2004) 1273–1289.
[17] R. Glowinski, T.W. Pan, T.I. Hesla, D.D. Joseph, J. Periaux, A fictitious domain approach to the direct numerical simulation of incompressible viscous flow past moving rigid bodies: Application to particulate flow, J. Comput. Phys. 169 (1) (2001) 363–427.
[18] C.S. Peskin, Numerical analysis of blood flow in the heart, J. Comp. Phys. 25 (3) (1977) 220–252.
[19] D.L. Youngs, K.W. Morton, M.J. Baines, Time-dependent multimaterial flow with large fluid distortion, in: Numerical Methods for Fluid Dynamics, New York, Academic Press, 1982.
[20] M. Fortin, R. Glowinski, Méthode de lagrangien augmenté. Application à la résolution numérique des problèmes aux limites, Collection méthodes mathématiques de l'informatique, Dunod, Paris, 1982.
[21] H.A. van der Vorst, BI–CGSTAB: A fast and smoothly converging variant of BI–CG for the solution of nonsymmetric linear systems, SIAM J. Sci. Stat. Comput. 13 (2) (1992) 631–644.